Membrane Binding Kinetics of Protein Kinase C βII Mediated by the C2 Domain[†]

Eric A. Nalefski[‡] and Alexandra C. Newton*

Department of Pharmacology, University of California at San Diego, La Jolla, California 92093-0640

Received April 16, 2001; Revised Manuscript Received August 30, 2001

ABSTRACT: Conventional isoforms of protein kinase C (PKC) are activated when their two membrane-targeting modules, the C1 and C2 domains, bind the second messengers diacylglycerol (DG) and Ca^{2+}, respectively. This study investigates the mechanism of Ca^{2+}-induced binding of PKC βII to anionic membranes mediated by the C2 domain. Stopped-flow fluorescence spectroscopy reveals that Ca^{2+}-induced binding of the isolated C2 domain to anionic vesicles proceeds via at least two steps: (1) rapid binding of two or more Ca^{2+} ions to the free domain with relatively low affinity and (2) diffusion-controlled association of the Ca^{2+}-occupied domain with vesicles. Ca^{2+} increases the affinity of the C2 domain for anionic membranes by both decreasing the dissociation rate constant (k_{off}) and increasing the association rate constant (k_{on}) for membrane binding. For binding to vesicles containing 40 mol % anionic lipid in the presence of 200 μM Ca^{2+}, k_{off} and k_{on} are 8.9 s^{-1} and 1.2×10^{10} M^{-1} s^{-1}, respectively. The k_{off} value increases to 150 s^{-1} when free Ca^{2+} levels are rapidly reduced, decreasing the average lifetime of the membrane-bound C2 domain ($\tau = k_{off}^{-1}$) from 110 ms in the presence of Ca^{2+} to 6.7 ms when Ca^{2+} is rapidly removed. Experiments addressing the role of electrostatic interactions reveal that they stabilize either the initial C2 domain−membrane encounter complex or the high-affinity membrane-bound complex. Specifically, lowering the phosphatidylserine mole fraction or including $MgCl_2$ in the binding reaction decreases the affinity of the C2 domain for anionic vesicles by both reducing k_{on} and increasing k_{off} measured in the presence of 200 μM Ca^{2+}. These species do not affect the k_{off} value when Ca^{2+} is rapidly removed. Studies with PKC βII reveal that Ca^{2+}-induced binding to membranes by the full-length protein proceeds minimally via two kinetically resolvable steps: (1) a rapid bimolecular association of the enzyme with vesicles near the diffusion-controlled limit and, most likely, (2) subsequent conformational changes of the membrane-bound enzyme. As is the case for the C2 domain, k_{off} for full-length PKC βII increases when Ca^{2+} is rapidly removed, reducing τ from 11 s in the presence of Ca^{2+} to 48 ms in its absence. Thus, both the C2 domain and the slow conformational change prolong the lifetime of the PKC βII−membrane ternary complex in the presence of Ca^{2+}, with rapid membrane release triggered by removal of Ca^{2+}. These results provide a molecular basis for cofactor regulation of PKC whereby the C2 domain searches three-dimensional space at the diffusion-controlled limit to target PKC to relatively common anionic phospholipids, whereupon a two-dimensional search is initiated by the C1 domain for the more rare, membrane-partitioned DG.

Reversible membrane translocation triggered by second messengers provides a highly efficient mechanism for the spatial and temporal control of signal-transducing proteins. Binding of soluble or membrane-bound second messengers to such proteins triggers their recruitment to specific membrane locations, poising them near their substrates and, in most cases, promoting activating conformational changes. Nature has perfected a library of membrane-targeting modules that are used alone, or, in many cases, in combination, to recruit proteins to the membrane following stimulus-dependent generation of specific ligands (*1*). In fact, the coordinated use of two membrane-targeting modules allows ultrasensitivity and increased specificity in responding to extracellular signals (*2*).

Protein kinase C (PKC)[1] family members serve as a paradigm for the reversible regulation of protein function by two membrane-targeting modules (*2*). In particular, the conventional isozymes are regulated by a C1 domain, which binds diacylglycerol (DG), and a C2 domain that binds Ca^{2+}. Generation of these two second messengers drives PKC from the cytosol to the membrane, where an additional interaction with phosphatidylserine (PS) results in a conformational change that releases an autoinhibitory (pseudosubstrate) sequence from the substrate-binding cavity, allowing substrate phosphorylation and downstream signaling. Extensive biochemical and biophysical analyses in vitro have revealed that PKC can be recruited to membranes by the C1 or the C2 domain alone (*3*). However, the binding energy supplied by engaging one domain on the membrane is typically too

[1] Abbreviations: PKC, protein kinase C; DG, diacylglycerol; PS, phosphatidylserine; PC, phosphatidylcholine; dansyl-PE and dPE, *N*-[5-(dimethylamino)naphthalene-1-sulfonyl]-1,2-dihexadecanoyl-*sn*-glycero-3-phosphoethanolamine; HEPES, *N*-(2-hydroxyethyl)piperazine-*N'*-2-ethanesulfonic acid; DTT, dithiothreitol; GST, glutathione *S*-transferase; FRET, fluorescence resonance energy transfer; EDTA, ethylene-diaminetetraacetic acid; EGTA, ethylene glycol bis(2-aminoethyl)-*N,N,N',N'*-tetraacetic acid.

low to displace the pseudosubstrate and activate PKC. Rather, both domains must be engaged on the membrane to provide the energy to release the pseudosubstrate from the substrate-binding cavity. Thus, high-affinity membrane binding is achieved by having both domains tethered to the membrane. This interaction is also readily reversed upon metabolism of DG, the C1 domain ligand, or decreases in intracellular Ca^{2+}, the C2 domain ligand. The use of two membrane-binding domains confers added specificity and sensitivity to signaling by conventional PKCs; these isozymes become activated only when both DG and Ca^{2+} signals are simultaneously on, with steep activation−deactivation kinetics resulting from the coordinated binding of two domains to the membrane.

The kinetics of translocation of PKC in cells in response to natural agonists have recently been captured using green fluorescent protein-tagged constructs of PKC (4−10). Agonist-stimulated translocation is rapid, typically occurring within 10 s, and short-lived, with redistribution to the cytosol within 5 min. The nature and magnitude of changes in Ca^{2+} and DG levels are both stimulus- and cell-specific. For example, both second messengers undergo oscillatory changes in response to some signals or rise transiently and then return to baseline levels in response to others (11, 12). As a consequence, PKC translocation has been reported to be sustained, oscillatory, or transient, depending on the isozyme, cell type, and stimulus (4−10). Understanding the complex mechanisms of translocation of PKC in vivo depends on understanding the kinetics and mechanisms of translocation of the isolated membrane-targeting modules.

Here we provide a detailed kinetic analysis of the regulation of PKC βII by the C2 domain. Specifically, we use stopped-flow spectroscopy to determine the association and dissociation rate constants for membrane binding by the isolated C2 domain of PKC β as well as the full-length PKC βII. Our results converge upon a model whereby Ca^{2+} targets PKC from three-dimensional space to the membrane via the C2 domain, allowing the enzyme's C1 domain to initiate a two-dimensional search for DG.

MATERIALS AND METHODS

Reagents. Synthetic phosphatidylcholine (PC), 1-palmitoyl-2-oleoyl-*sn*-glycero-3-phosphocholine, and PS, 1-palmitoyl-2-oleoyl-*sn*-glycero-3-phosphoserine, were purchased from Avanti Polar Lipids. The danyslated phospholipid *N*-[5-(dimethylamino)naphthalene-1-sulfonyl]-1,2-dihexadecanoyl-*sn*-glycero-3-phosphoethanolamine (dPE) was purchased from Molecular Probes. Large unilamellar phosholipid vesicles 100 nm in diameter were prepared by extruding rehydrated phospholipid suspensions through two stacked 0.1 μm polycarbonate membranes (13). The phospholipid concentration ([L]) was determined by assaying the phosphorus content as described previously (14), and the vesicle concentration ([v]) was calculated assuming 90 000 lipids per vesicle (15). All experiments were carried out at 25 °C in standard assay buffer composed of 150 mM NaCl, 20 mM *N*-(2-hydroxyethyl)piperazine-*N*′-2-ethanesulfonic acid (HEPES) (pH 7.4), and 1 mM dithiothreitol (DTT), supplemented with $CaCl_2$ and $MgCl_2$ as indicated. Buffers and plastic ware were decalcified as described in ref 16.

Protein Purification. The C2 domain of rat PKC βII was expressed as a glutathione *S*-transferase (GST) fusion protein

in *Escherichia coli* (3). The isolated C2 domain was liberated by thrombin digestion, purified away from GST to homogeneity by size exclusion chromatography, and quantified by UV absorbance using its calculated molar extinction coefficient (17). Full-length rat PKC βII was expressed in insect cells, purified to homogeneity as described previously (18), and quantified by comparing its silver staining intensity in SDS−PAGE gels to that of a bovine serum albumin standard.

Fluorescence Spectroscopy of Transient Kinetic Processes. Kinetic measurements were carried out on an Applied Photophysics π*−180 stopped-flow fluorescence spectrophotometer (Leatherhead, U.K.). The mixing time of the instrument was ∼2 ms, determined using a colorimetric chemical reaction (19). Hence, data collected in the first 2 ms were excluded from analysis. Intrinsic tryptophan emission was monitored using 280 nm excitation light and by recording emission through a 325 nm high-pass filter. Protein-to-membrane fluorescence resonance energy transfer (FRET) was monitored using 280 nm excitation light and by recording dansyl emission through a 465 nm high-pass filter. Details of the individual experiments are given in the figure legends. For each time course, five traces were collected, averaged, and subjected to nonlinear, least-squares curve fitting using the KaleidaGraph software package (version 3.08). Fluorescence time courses were analyzed with exponential equations of the general form

$$F(t) = F_0 + \sum_{i=1}^{n} A_{\text{obs}(i)} e^{-k_{\text{obs}(i)}t} \tag{1}$$

where $F(t)$ represents the observed fluorescence at time t, F_0 is a fluorescence offset representing the final fluorescence, and $A_{\text{obs}(i)}$ represents the amplitude and $k_{\text{obs}(i)}$ the observed rate constant for the ith of n phases. Time courses are presented either as offset fluorescence emission in arbitrary milliunits (mU) or as offset emission relative to the amplitude. For graphical clarity, only a fraction of the total data collected in each time course is represented. Observed rate constants and amplitudes were subjected to weighted least-squares analysis (20) as described below, justification for which is provided in the Results.

For the monophasic time courses of reversible C2 domain binding to vesicles carried out under pseudo-first-order conditions, the observed rate constants were plotted as a function of [v] and fitted with the linear equation

$$k_{\text{obs}} = k_{\text{on}}[v] + k_{\text{off}} \tag{2}$$

where k_{on} represents the apparent second-order rate constant and k_{off} represents the apparent dissociation rate constant. The ratio of k_{off} to k_{on} provides the calculated apparent vesicle dissociation constant (K_d^{calc}). Absolute values of the observed amplitudes (A_{obs}) were plotted as a function of [v] and fitted with the hyperbolic equation

$$A_{\text{obs}} = A_{\text{max}} \left(\frac{[v]}{[v] + K_d^{\text{obs}}} \right) \tag{3}$$

where A_{max} represents the calculated maximal amplitude and K_d^{obs} represents the observed vesicle dissociation constant. For the biphasic time courses of PKC βII binding to vesicles,

$k_{obs(1)}$ of the fast phase was plotted as a function of [v] and fitted with the linear equation

$$k_{obs(1)} = k_1[v] + C \qquad (4)$$

where k_1 represents the apparent second-order rate constant for the bimolecular step and C is a constant equaling the y-intercept. The y-intercept represents the sum $k_{-1} + k_2 + k_{-2}$, where k_{-1} equals the apparent dissociation rate constant for the bimolecular step and $k_2 + k_{-2}$ is the sum of the forward and reverse rate constants for a first-order transition step. For the slow phase of PKC βII binding to vesicles, $k_{obs(2)}$ was plotted as a function of [v] and fitted with a hyperbolic equation

$$k_{obs(2)} = k_{max(2)}\left(\frac{[v]}{[v] + C}\right) \qquad (5)$$

where C is a constant and $k_{max(2)}$ represents the calculated asymptote, which is equal to the sum $k_2 + k_{-2}$. For PKC βII, the total observed amplitudes of the slow and fast phases were analyzed with eq 3 to obtain the net apparent dissociation constant $[K_{d(net)}^{obs}]$.

The observed rate constant for the monophasic time course of C2 domain trapping by unlabeled anionic vesicles equals the membrane dissociation rate constant k_{off} in 200 μM Ca^{2+}. The observed rate constants $[k_{off(1)}$ and $k_{off(2)}]$ for biphasic PKC βII trapping represent rate constants for two slow phases. The membrane dissociation rate constant of PKC βII was taken as $k_{off(1)}$, since control experiments demonstrated that only the fast phase represents a fluorescence change associated with dissociation triggered by unlabeled vesicles (see the Results). For the monophasic time course of irreversible membrane dissociation by the C2 domain or PKC βII initiated by rapid mixing with Ca^{2+} chelators, the observed rate constant k_{off} equals the apparent rate constant for disassembly of ternary complexes at low Ca^{2+} concentrations.

Fluorescence Spectroscopy of Steady-State Equilibrium Processes. Intrinsic tryptophan emission of the C2 domain (0.5 μM) was monitored on a Jobin (Edison, NJ) Yvon-SPEX FluroMax-2 fluorescence spectrophotometer using 280 nm excitation light and by recording emission at 340 nm in standard buffer at 25 °C. The observed fluorescence change (ΔF_{obs}) was plotted as a function of free Ca^{2+} concentration (x) and fitted with a modified Hill equation (*16*):

$$\Delta F_{obs} = \Delta F_{max}\left[\frac{x^{n_H}}{x^{n_H} + ([Ca^{2+}]_{1/2})^{n_H}}\right] \qquad (6)$$

where ΔF_{max} represents the calculated maximal fluorescence change, n_H represents an apparent Hill constant, and $[Ca^{2+}]_{1/2}$ is equal to the Ca^{2+} concentration at the midpoint in the titration, an approximation of the average Ca^{2+} dissociation constant. Since $[Ca^{2+}]_{1/2}$ was considerably greater than the protein concentration, the concentration of total Ca^{2+} was taken as the free concentration.

RESULTS

Ca^{2+} Binding to the Free C2 Domain. Functional studies have demonstrated that three Ca^{2+} ions bind to the PKC β C2 domain−membrane ternary complex (*17*). Tryptophan
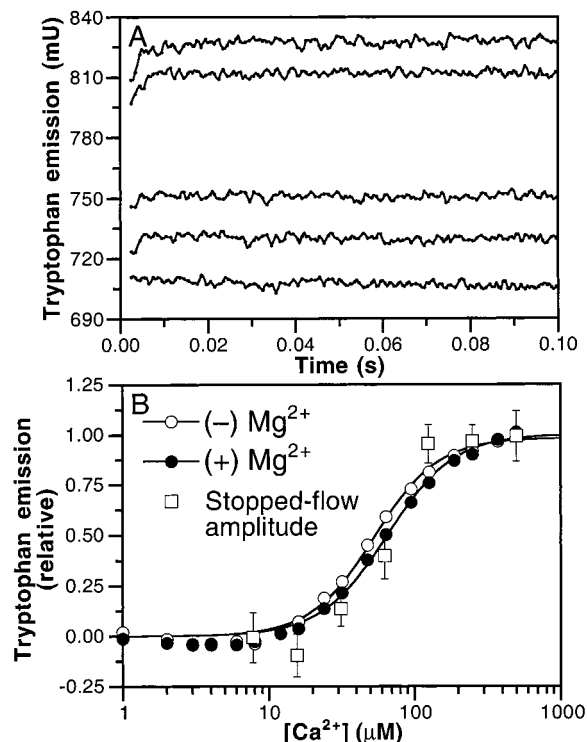

FIGURE 1: Kinetics and equilibrium of Ca^{2+} binding to the free PKC β C2 domain. The C2 domain (0.5 μM) was mixed with increasing concentrations of $CaCl_2$ either by stopped-flow methods or by sequential additions. Tryptophan emission was recorded. (A) Representative traces showing the time course of tryptophan emission changes for the C2 domain mixed by stopped-flow methods with 8−500 μM (final) $CaCl_2$ (from bottom to top). (B) Dependence of the increase in tryptophan emission on Ca^{2+} concentration. Increases in tryptophan emission observed by stopped-flow methods (□) or by sequential additions to a given sample (● and ○) were normalized to the maximal calculated change in emission intensity. Bars represent standard deviations of three stopped-flow determinations. Solid lines through titration data represent fits with the modified Hill equation (eq 6), which yielded the following apparent equilibrium parameters: $[Ca^{2+}]_{1/2} = 55 \pm 2$ μM, $n_H = 1.9 \pm 0.1$, (−) Mg^{2+} (○); and $[Ca^{2+}]_{1/2} = 65 \pm 3$ μM, $n_H = 1.9 \pm 0.1$, (+) 5 mM Mg^{2+} (●). Fitting stopped-flow amplitudes with the Hill equation (not shown) yielded a $[Ca^{2+}]_{1/2}$ value of 68 ± 6 μM.

fluorescence of the PKC β C2 domain was monitored to examine the kinetic and equilibrium parameters of Ca^{2+} binding to the C2 domain in the absence of membranes. Ca^{2+} binding to this C2 domain induces an increase in tryptophan emission intensity (*17*), indicating that Ca^{2+} binding causes environmental changes proximal to at least one of its four tryptophans. Rapidly mixing the C2 domain via stopped-flow methods with solutions containing increasing Ca^{2+} concentrations increased the tryptophan emission intensity (Figure 1A). The fluorescence changes were completed during the mixing time of the instrument ($\sim$2 ms), indicating that the Ca^{2+} binding reaction reaches equilibrium rapidly. Thus, the rate constants for Ca^{2+} binding to the C2 domain must be very large (see the Discussion). The Ca^{2+} dependence of the normalized amplitudes measured by stopped-flow methods was very similar to that obtained independently by sequentially titrating Ca^{2+} into a solution containing the C2 domain (Figure 1B); both plots were sigmoidal and had similar midpoints (68 and 55 μM, respectively), comparable to previously reported values (*17*). In addition, the apparent Hill coefficients were larger than 1 (n_H = 1.9), indicating

that the membrane-free PKC β C2 domain binds at least two Ca^{2+} ions very rapidly in solution.

Attempts were made to measure the rate constant for Ca^{2+} dissociation from the C2 domain in the absence of membranes by monitoring intrinsic tryptophan emission. When the Ca^{2+}-bound, membrane-free C2 domain was rapidly mixed with EDTA, the time course of loss of tryptophan emission intensity was completed during the mixing time of the stopped-flow instrument (data not shown), suggesting that the rate constant for Ca^{2+} dissociation is very large ($\gg 500$ s^{-1}), in agreement with previous observations (*17*).

Membrane Binding Kinetic and Equilibrium Constants of the Isolated C2 Domain. Tryptophan emission was further employed to measure the rate constants for vesicle association and dissociation, since additional increases in tryptophan emission intensity are observed when the PKC β C2 domain binds vesicles (*17*). Rapidly mixing the C2 domain, preincubated in Ca^{2+}, with anionic vesicles resulted in a monophasic increase in tryptophan emission intensity (Figure 2A). This fluorescence increase required the presence of Ca^{2+} (data not shown). The observed rate constant for the approach to equilibrium was linearly dependent on vesicle concentration and showed no sign of curvature even at high vesicle concentrations (Figure 2B). Since this experiment was carried out using concentrations of anionic phospholipids that greatly exceeded that of the C2 domain and hence remained effectively constant throughout the time course, the binding reaction can be considered pseudo-first-order with respect to phospholipid. The *y*-intercept provided an estimate of the apparent dissociation rate constant (k_{off}) equal to 7.2 s^{-1}, and the slope provided the apparent second-order association rate constant (k_{on}) equal to 1.3×10^{10} M^{-1} s^{-1} (Table 1). The ratio of these kinetic parameters provided an estimate of the apparent vesicle dissociation constant (K_d^{calc}) equal to 0.53 nM. In addition, the observed amplitudes were hyperbolically dependent on vesicle concentration (Figure 2C) and yielded an observed vesicle dissociation constant (K_d^{obs}) equal to 0.39 nM, which is similar to that calculated from the ratio of kinetic parameters (Table 1).

Fluorescence resonance energy transfer (FRET) from tryptophans in the C2 domain to trace amounts of dansylated phospholipids incorporated into PS/PC vesicles was employed to further measure the kinetics of vesicle binding (*17*). As in Figure 2, the resulting time courses were monophasic over a wide range of vesicle concentrations (Figure 3A). The fluorescence increase required the presence of Ca^{2+} (data not shown), suggesting that the intrinsic membrane affinity of the Ca^{2+}-free C2 domain is small ($K_d \gg 2.4$ nM). From five independent experiments, the linear dependence of k_{obs} on vesicle concentration (Figure 3B) yielded a k_{off} value equal to 8.9 s^{-1} and a k_{on} value equal to 1.2×10^{10} M^{-1} s^{-1}, as summarized in Table 1. Both parameters agree quite well with the values obtained from the previous approach employing tryptophan emission. Moreover, these kinetic parameters yielded a K_d^{calc} value equal to 0.73 nM, which is similar to the K_d^{obs} of 0.40 nM determined from the hyperbolic dependence of observed amplitudes on vesicle concentration (Figure 3C). The scarcity of data well above the K_d value is likely to account for the small discrepancy between these two latter values.
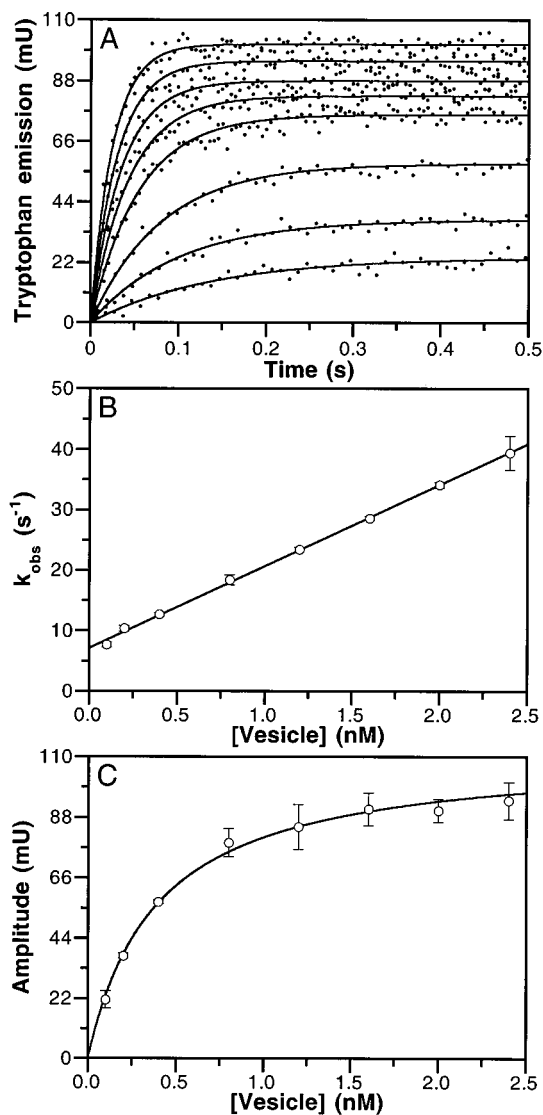

FIGURE 2: Kinetics of Ca^{2+}-induced binding of the C2 domain to anionic phospholipid vesicles measured by monitoring intrinsic tryptophan fluorescence. The C2 domain (0.5 μM) in Ca^{2+} (200 μM) was rapidly mixed with an equal volume of increasing concentrations of PS/PC (40:60) vesicles in Ca^{2+} (200 μM). Intrinsic tryptophan emission was recorded. (A) Representative traces showing the time course of tryptophan emission increases for the C2 domain mixed with 0.1–2.4 nM (final) vesicles (from bottom to top). Solid lines show monoexponential fits, which yielded k_{obs} values and amplitudes. (B) Dependence of k_{obs} on vesicle concentration. Bars represent the standard deviations of three determinations from a single experiment; the solid line shows a weighted linear fit (eq 2). The *y*-intercept provided the dissociation rate constant k_{off}, and the slope yielded the association rate constant k_{on}. The ratio of these kinetic parameters provided the K_d^{calc}. (C) Dependence of the observed amplitude on vesicle concentration. Bars represent standard deviations of three determinations from a single experiment; the solid line shows a weighted hyperbolic fit (eq 3), which yielded the K_d^{obs} value. Results are summarized in Table 1.

At a final concentration of 200 μM Ca^{2+}, the observed rate constant of vesicle binding was independent of whether the Ca^{2+} was preincubated with the C2 domain prior to mixing with vesicles or added at the same time as vesicles (data not shown). This observation reflects the fact that Ca^{2+} binding to the C2 domain is a rapid equilibrium and that under these conditions, Ca^{2+} binding steps are not rate-limiting.

Table 1: Equilibrium and Kinetic Parameters of Ca^{2+}-Induced Binding to Anionic Membranes by the Isolated PKC β C2 Domain

| | high Ca^{2+} [a] | | | | low Ca^{2+} [b] |
assay	k_{on} ($\times 10^{10}$ M^{-1} s^{-1})	k_{off} (s^{-1})	K_d^{calc} (nM)	K_d^{obs} (nM)	k_{off} (s^{-1})
intrinsic fluorescence	1.35 ± 0.02	7.2 ± 0.2	0.53 ± 0.02	0.39 ± 0.03	149 ± 2
FRET	1.214 ± 0.006	8.89 ± 0.02	0.732 ± 0.004	0.400 ± 0.005	156 ± 2

[a] Weighted, least-squares value, where intrinsic tryptophan emission of C2 domain binding to PS/PC vesicles (40:60) was monitored (Figure 2), or weighted averages of five independent experiments, where protein-to-membrane FRET resulting from C2 domain binding to PS/PC/dPE (35:60:5) vesicles was monitored (Figure 3). k_{on} is taken from the slope and k_{off} from the y-intercept of the linear plot of k_{obs} vs vesicle concentration; K_d^{calc} is defined as the ratio of k_{off} to k_{on}. K_d^{obs} obtained from the hyperbolic dependence of A_{obs} on vesicle concentration. Experimental conditions: 25 °C, 150 mM NaCl, 20 mM HEPES (pH 7.4), 1 mM DTT, and 200 μM $CaCl_2$. [b] Average ($\pm$standard error of the mean) from the Ca^{2+} trapping approach using PS/PC (40:60) vesicles ($n = 3$) or PS/PC/dPE (35:60:5) vesicles ($n = 12$) (Figure 4). Experimental conditions (after mixing): 25 °C, 150 mM NaCl, 20 mM HEPES (pH 7.4), 2.5 mM EDTA, 1 mM DTT, 100 μM $CaCl_2$, and 2.4 nM vesicles.

Apparent Membrane Dissociation Rate Constants of the C2 Domain. A "protein trapping" approach (15) was developed to directly measure the apparent rate constant for membrane dissociation of the PKC β C2 domain in the presence of 200 μM bulk Ca^{2+}. A solution containing the C2 domain preincubated with PS/PC/dPE vesicles and Ca^{2+} was rapidly mixed with a solution containing Ca^{2+} and a large molar excess of unlabeled PS/PC vesicles to trap the C2 domain after its dissociation from the fluorescent target vesicles. By monitoring the loss in the protein-to-membrane FRET signal, we directly measured the apparent rate constant for dissociation from the PS/PC/dPE vesicles. A monophasic loss in the protein-to-membrane FRET signal was observed with a rate constant of 9.2 s^{-1} (Figure 4A), which was independent of the concentration of trapping PS/PC vesicles (data not shown). The loss in the FRET signal required the presence of Ca^{2+} (data not shown), indicating that this approach monitors the dissociation of a Ca^{2+}-induced process. Importantly, this rate constant was very close to the value of 8.9 s^{-1} that was calculated above by extrapolation to the y-intercept (Figure 3B and Table 1). Therefore, in the presence of 200 μM Ca^{2+}, the average lifetime of the C2 domain–membrane ternary complex is 110 ms ($\tau = k_{off}^{-1} = 1/8.9$ s^{-1}).

A "Ca^{2+} trapping" approach was then employed to measure the apparent rate constant for membrane dissociation of the PKC β C2 domain in the presence of a very low concentration of Ca^{2+} (21). A solution containing the C2 domain preincubated with target anionic vesicles and Ca^{2+} was mixed via stopped-flow methods with a solution containing a large molar excess of EDTA to rapidly trap free Ca^{2+} ions present immediately after the mixing step and after their dissociation from the C2 domain. Rate constants were determined by monitoring the loss in intrinsic tryptophan emission when PS/PC target vesicles were employed and by monitoring the loss in the protein-to-membrane FRET signal when PS/PC/dPE target vesicles were employed (Figure 4B). In both cases, a monophasic loss in fluorescence was observed; when intrinsic fluorescence was monitored, a rate constant equal to 149 s^{-1} was observed, and when protein-to-membrane FRET was observed, a comparable rate constant equal to 156 s^{-1} was observed (Table 1). The similarity in these two values suggests that they represent constants governing the same rate-limiting step in chelator-induced membrane dissociation. Importantly, the rate constant for this step, which represents the apparent rate constant for membrane dissociation of the C2 domain in the presence of a very low concentration of Ca^{2+}, is nearly 20-fold larger

than the apparent vesicle dissociation constant of 8.9 s^{-1} calculated above by extrapolation (Figure 3B and Table 1) or 9.2 s^{-1}, measured by C2 domain trapping (Figure 4A) in the presence of 200 μM Ca^{2+}. In other words, the average lifetime of the C2 domain–membrane ternary complex is only 6.7 ms when Ca^{2+} levels are rapidly lowered ($\tau = k_{off}^{-1} = 1/150$ s^{-1}) but is 110 ms in the presence of 200 μM Ca^{2+} (see above).

Effect of Ca^{2+} on C2 Domain Equilibrium and Kinetic Constants. The effect of the concentration of Ca^{2+} itself on C2 domain binding to membranes was tested (Figure 5). When the bulk concentration of Ca^{2+} was reduced to 50 μM and PS/PC/dPE (35:60:5) vesicles were employed, the k_{off} value increased to 16 s^{-1} and the k_{on} value decreased to 0.73 $\times 10^{10}$ M^{-1} s^{-1} (Figure 5A). As expected, the K_d^{calc} value increased with this reduced Ca^{2+} concentration (Figure 5A), resulting in a dissociation constant equal to 2.2 nM that was consistent with the K_d^{obs} value based on analysis of the observed amplitudes.

The effect of Ca^{2+} on membrane affinity and kinetics was further investigated by testing the Ca^{2+} concentration dependence of the rate constant for C2 domain binding to a fixed concentration of PS/PC/dPE (35:60:5) vesicles. The plot of k_{obs} versus Ca^{2+} concentration was biphasic (Figure 5B); k_{obs} decreased with increasing Ca^{2+} concentrations up to approximately 40 μM Ca^{2+}, whereupon k_{obs} then increased and approached a maximum by 200 μM Ca^{2+}. Analysis of the Ca^{2+} dependence of the observed amplitudes confirmed that the membrane affinity increased with increasing Ca^{2+} concentration, yielding a midpoint at approximately 33 μM Ca^{2+} (Figure 5C). The apparent Hill coefficient was equal to 2.3, indicating that at least two Ca^{2+} ions are required to induce membrane docking. These results indicate that, under these conditions, at Ca^{2+} concentrations below ~40 μM, the increase in membrane affinity of the C2 domain induced by Ca^{2+} can be attributed to a sharp decrease in the apparent dissociation rate constant. In contrast, above ~40 μM Ca^{2+}, the increase in membrane affinity can be attributed to an increase in the apparent association rate constant that approaches a maximum. Therefore, Ca^{2+} levels modulate the apparent membrane affinity of the PKC β C2 domain by both increasing k_{on} and decreasing k_{off}.

Effect of the PS Mole Fraction on C2 Domain Kinetic and Equilibrium Constants. The effect of increasing the PS mole fraction in target vesicles was tested, since increasing anionic content raises the affinity of PKC and its isolated C2 domain for vesicles (3, 22). For all three mole fractions that were
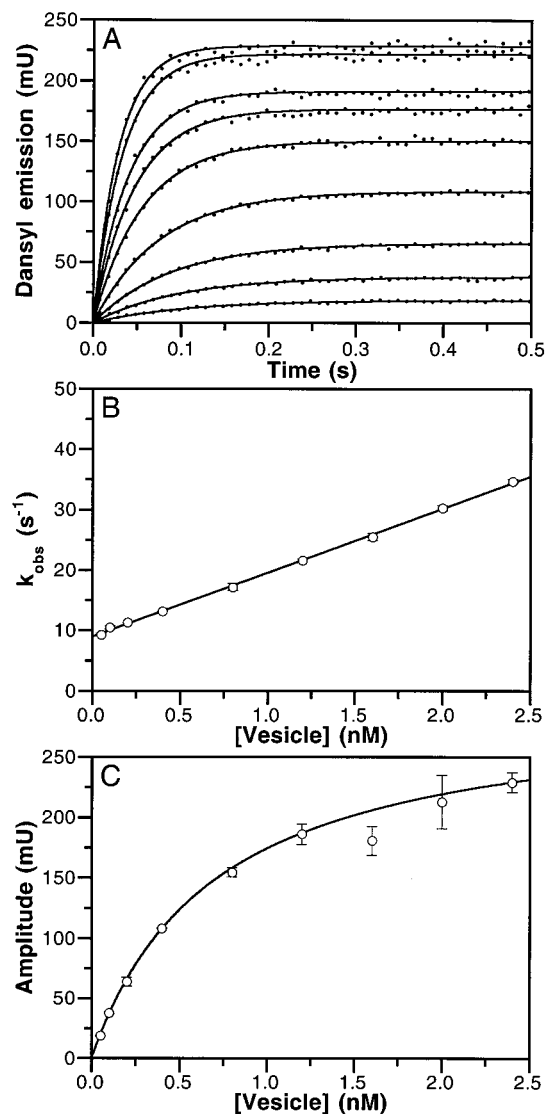
FIGURE 3: Kinetics of Ca^{2+}-induced C2 domain binding to anionic phospholipid vesicles measured by monitoring the protein-to-membrane FRET signal. The C2 domain (0.5 μM) in Ca^{2+} (200 μM) was rapidly mixed with an equal volume of increasing concentrations of PS/PC/dPE (35:60:5) vesicles in Ca^{2+} (200 μM). Tryptophan in the C2 domain was excited, and dansyl emission from vesicles was recorded. (A) Representative traces showing the time course of dansyl emission increases for the C2 domain mixed with 0.05−2.4 nM (final) anionic vesicles (from bottom to top). Solid lines show monoexponential fits, which yielded k_{obs} values and amplitudes. (B) Dependence of k_{obs} on vesicle concentration. Bars represent standard deviations of three determinations from a single experiment; the solid line shows a weighted linear fit (eq 2). The y-intercept yielded the k_{off} value; the slope yielded the k_{on} value, and their ratio provided the K_d^{calc} value. (C) Dependence of the observed amplitude on vesicle concentration. Bars represent standard deviations of three determinations from a single experiment; the solid line shows a weighted hyperbolic fit (eq 3), which yielded the K_d^{obs} value. Results of five independent experiments are averaged in Table 1.

tested (25, 35, and 45%), the observed time courses of membrane binding were monophasic at all vesicle concentrations (data not shown), and the resulting k_{obs} values were linearly dependent on vesicle concentration without signs of curvature (Figure 6A). As the PS mole fraction increased from 25 to 35 to 45, k_{off} decreased from 18 to 8.9 to 4.0 s^{-1}, respectively (Table 2). Concomitantly, k_{on} increased from 0.80×10^{10} to 1.2×10^{10} to 2.1×10^{10} M^{-1} s^{-1}, respectively,
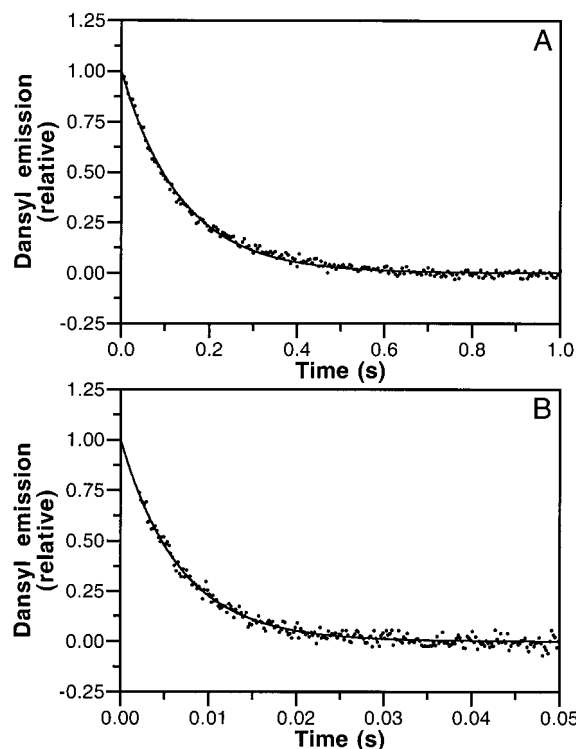

FIGURE 4: Membrane dissociation kinetics of the C2 domain measured by trapping. (A) Dissociation kinetics measured by C2 domain trapping. The C2 domain (1.5 μM) preincubated with Ca^{2+} (200 μM) and labeled anionic PS/PC/dPE (35:60:5) vesicles (0.2 nM) was rapidly mixed with an equal volume of unlabeled PS/PC (40:60) vesicles (5 nM) in Ca^{2+} (200 μM). Tryptophan was excited, and dansyl emission from vesicles was recorded. Shown is a representative trace of the time-dependent decrease in dansyl emission, normalized to the calculated maximal fluorescence change. The solid line shows a monoexponential fit, which yielded an average ($\pm$standard error of the mean) k_{off} value equal to 9.2 $\pm$ 0.4 s^{-1} ($n = 7$). This value is comparable to the extrapolated k_{off} value of 8.9 s^{-1} (Table 1). Control experiments showed that the decreases in dansyl emission that were observed required the presence of the C2 domain and the presence of PS/PC/dPE vesicles and were eliminated by the presence of 1 mM EDTA (data not shown). Similar observed rate constants were obtained when different concentrations of trapping PS/PC vesicles were employed (data not shown). (B) Dissociation kinetics measured by Ca^{2+} trapping. The C2 domain (0.5 μM), Ca^{2+} (200 μM), and PS/PC/dPE (35:60:5) vesicles (4.8 nM) were rapidly mixed with an equal volume of EDTA (5 mM). Tryptophan was excited, and dansyl emission from vesicles was recorded. Representative trace showing the time course of loss of dansyl emission normalized to the calculated maximal fluorescence change. The solid line shows a monoexponential fit, which yielded k_{off}. When PS/PC (40:60) vesicles were employed and tryptophan emission was monitored, similar results were obtained. Results are summarized in Table 1.

and K_d^{calc} values based on kinetic parameters decreased from 2.3 to 0.76 to 0.20 nM, respectively (Table 2). As before, there was close agreement between K_d^{calc} values and K_d^{obs} values derived from the hyperbolic dependence of the observed amplitudes on vesicle concentration; the latter values also decreased, from 2.4 to 0.55 to 0.25 nM, as the PS mole fraction increased (Table 2). These results indicate that as the anionic phospholipid content is raised in the target vesicles, the membrane binding affinity of the PKC β C2 domain is elevated because of both increases in k_{on} and decreases in k_{off}.

The Ca^{2+} trapping approach was employed to measure the effect of PS mole fraction on the apparent membrane

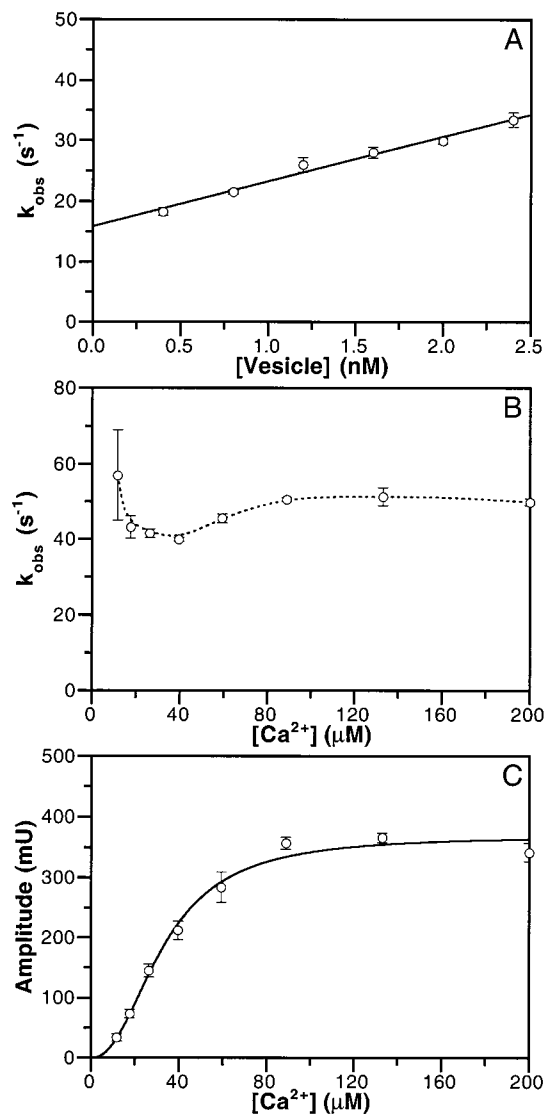FIGURE 5: Effect of Ca^{2+} concentration on anionic membrane binding kinetics of the C2 domain. (A) The C2 domain (0.5 μM) in Ca^{2+} (50 μM) was rapidly mixed with an equal volume of increasing concentrations of PS/PC/dPE (35:60:5) vesicles in Ca^{2+} (50 μM). Tryptophan was excited; dansyl emission from vesicles was recorded, and k_{obs} values and amplitudes were determined from monoexponential fits of time courses. Bars represent standard deviations of three determinations of k_{obs} from a single experiment; the solid line shows a weighted linear fit (eq 2). The value of k_{off} obtained from the y-intercept was 15.7 ± 0.5 s^{-1}, and the value of k_{on} obtained from the slope was (0.73 ± 0.04) × 10^{10} M^{-1} s^{-1}. The K_d^{calc} value from these kinetic parameters was 2.2 ± 0.3 nM. K_d^{obs} was estimated from the vesicle dependence of observed amplitudes to be ≥2.4 nM (data not shown). (B and C) The C2 domain (0.5 μM) was rapidly mixed with an equal volume of increasing concentrations of Ca^{2+} and a fixed concentration of PS/PC/dPE (35:60:5) vesicles (4.8 nM). Tryptophan was excited; dansyl emission from vesicles was recorded, and k_{obs} values and amplitudes were determined from monoexponential fits of time courses. Bars represent standard deviations of three determinations from a single experiment. The biphasic character of the dashed line (B) suggests two different effects of Ca^{2+} on k_{obs}. The solid line (C) shows a weighted fit to the modified Hill equation (eq 6), which yielded a $[Ca^{2+}]_{1/2}$ of 33 ± 2 μM and an n_H of 2.3 ± 0.3.

dissociation constant of the PKC β C2 domain when Ca^{2+} levels are rapidly lowered. When PS/PC/dPE target vesicles containing 25 or 45 mol % PS were employed, a rate constant equal to 138 or 133 s^{-1}, respectively, was observed (Table
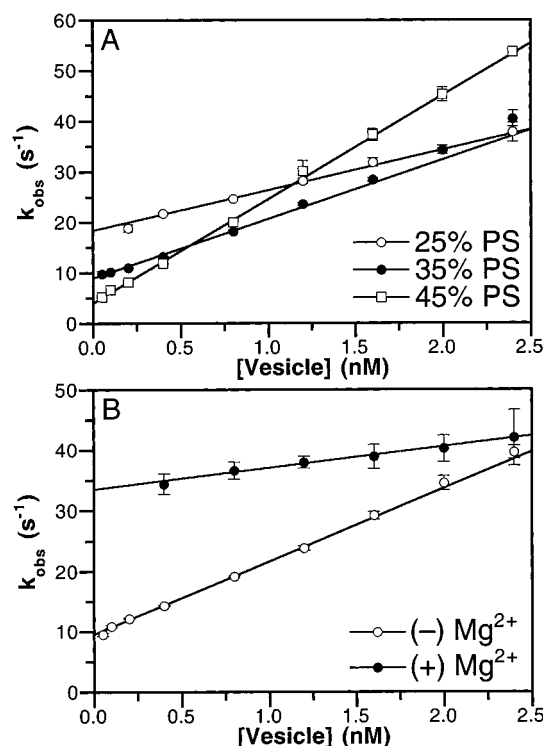

FIGURE 6: Effect of the PS mole fraction and Mg^{2+} concentration on the membrane binding kinetics of the C2 domain. (A) Effect of PS mole fraction. The C2 domain (0.5 μM) in Ca^{2+} (200 μM) was rapidly mixed with an equal volume of increasing concentrations of PS/PC/dPE vesicles in Ca^{2+} (200 μM). Vesicles were composed of the indicated percentages of PS, dPE at 5%, and PC to 100%. Tryptophan was excited; dansyl emission from vesicles was recorded, and k_{obs} values and amplitudes were determined from monoexponential fits of time courses. Solid lines show weighted linear fits (eq 2) of the plot of k_{obs} vs vesicle concentration; bars represent standard deviations of three determinations from a single experiment. Results are summarized in Table 2. (B) Effect of Mg^{2+} concentration. The C2 domain (0.5 μM) in Ca^{2+} (200 μM), with or without 5 mM $MgCl_2$, was rapidly mixed with an equal volume of increasing concentrations of PS/PC/dPE (35:60:5) vesicles in Ca^{2+} (200 μM) with (●) or without (○) $MgCl_2$. Tryptophan was excited; dansyl emission from vesicles was recorded, and k_{obs} values and amplitudes were determined from monoexponential fits of time courses. Solid lines show weighted linear fits (eq 2) of the plot of k_{obs} vs vesicle concentration; bars represent standard deviations of three determinations from a single experiment. Values determined in the presence of Mg^{2+} were as follows: k_{off} = 34 ± 2 s^{-1}, k_{on} = (0.35 ± 0.14) × 10^{10} M^{-1} s^{-1}, and K_d^{calc} = 10 ± 4 nM. The plot of observed amplitudes vs vesicle concentration indicated that K_d^{obs} is estimated to be >2.5 nM in the presence of Mg^{2+} (not shown).

2). These values are similar to the rate constant of 159 s^{-1} measured when 35 mol % PS was employed. These observations indicate that the PS mole fraction in the vesicles has little effect on the rate-limiting step in chelator-induced membrane dissociation of the PKC β C2 domain.

Effect of Mg^{2+} on C2 Domain Equilibrium and Kinetic Constants. The influence of $MgCl_2$ on C2 domain kinetics was tested, since this divalent cation decreases the affinity of full-length PKC and its isolated C2 domain for vesicles (3, 22). This effect has been ascribed to the ability of Mg^{2+} to reduce the magnitude of the membrane surface potential by accumulating nonspecifically near the membrane surface (22–24). When 5 mM $MgCl_2$ was present and PS/PC/dPE (35:60:5) vesicles were employed, the k_{off} value increased 4-fold to 34 s^{-1}, and the k_{on} value decreased 4-fold to 0.35

Table 2: Effect of Vesicle PS Composition on Equilibrium and Kinetic Parameters of Ca^{2+}-Induced Binding to Anionic Membranes by the Isolated PKC β C2 Domain[a]

	high Ca^{2+} [b]				low Ca^{2+} [c]
% PS	k_{on} ($\times 10^{10}$ M^{-1} s^{-1})	k_{off} (s^{-1})	K_d^{calc} (nM)	K_d^{obs} (nM)	k_{off} (s^{-1})
25	0.79 ± 0.02	18.4 ± 0.2	2.30 ± 0.07	2.4 ± 0.2	138 ± 1
35	1.17 ± 0.01	8.92 ± 0.02	0.760 ± 0.009	0.55 ± 0.01	159 ± 2
45	2.05 ± 0.01	4.02 ± 0.03	0.196 ± 0.002	0.25 ± 0.01	133 ± 1

[a] Vesicles composed of the indicated PS mole fraction, 5 mol % dPE, and the remainder PC. [b] Weighted, least-squares fit of data presented in Figure 6A. k_{on} is taken from the slope and k_{off} from the y-intercept of linear plot of k_{obs} vs vesicle concentration. K_d^{calc} is defined as the ratio of k_{off} to k_{on}. K_d^{obs} was obtained by a hyperbolic plot of A_{obs} vs vesicle concentration (data not shown). Experimental conditions: 25 °C, 150 mM NaCl, 20 mM HEPES (pH 7.4), 1 mM DTT, and 200 μM $CaCl_2$. [c] Average ($\pm$standard error of the mean) from the Ca^{2+} trapping approach ($n = 4$), carried out as described in the legend of Figure 4B. Experimental conditions (after mixing): 25 °C, 150 mM NaCl, 20 mM HEPES (pH 7.4), 2.5 mM EDTA, 1 mM DTT, 100 μM $CaCl_2$, and 2.4 nM vesicles.

$\times 10^{10}$ M^{-1} s^{-1} (Figure 6B). These changes yielded an elevated K_d^{calc} value equal to 10 nM, a 14-fold increase from 0.73 nM, which was measured in the absence of Mg^{2+}. This decrease in vesicle affinity in the presence of Mg^{2+} resulted in diminished amplitudes of the stopped-flow events, preventing accurate determination of the K_d^{obs} value by analysis of amplitudes (see the legend of Figure 6B).

In principle, the presence of Mg^{2+} might reduce the apparent second-order rate constant by reducing the apparent affinity of the C2 domain for Ca^{2+} (see the Discussion). However, since the presence of Mg^{2+} had no effect on the apparent affinity of the membrane-free C2 domain for Ca^{2+} (Figure 1B), under these conditions Mg^{2+} does not directly compete for the two or more Ca^{2+} ions that bind to this domain and induce environmental changes. Thus, as did decreasing the anionic content of the vesicle, the presence of Mg^{2+} reduces the membrane binding affinity of the PKC β C2 domain by both decreasing k_{on} and increasing k_{off}.

The Ca^{2+} trapping approach was employed to measure the effect of $MgCl_2$ on the apparent membrane dissociation rate constant of the PKC β C2 domain when Ca^{2+} levels are rapidly lowered. First, the chelator EDTA was replaced with EGTA to permit Ca^{2+} chelation in the presence of Mg^{2+}. As expected, the use of EGTA had little effect on the observed time course; a rate constant equal to 149 ± 4 s^{-1} ($n = 4$) was observed (data not shown), which is very similar to the value of 156 s^{-1} measured when EDTA was employed as the trapping agent (Figure 4B). Ca^{2+} chelation in the presence of 5 mM $MgCl_2$ by EGTA resulted in a slightly smaller rate constant equal to 120 ± 10 s^{-1} ($n = 4$) (data not shown). These observations indicate that, as was the case for the PS mole fraction in the vesicles, Mg^{2+} has little effect on the rate-limiting step in chelator-induced membrane dissociation of the PKC β C2 domain.

Membrane Binding Kinetic and Equilibrium Constants of Full-Length PKC βII. Protein-to-membrane FRET was employed to measure the kinetic and equilibrium constants for binding of full-length PKC βII to target anionic vesicles. Solutions containing PKC βII and Ca^{2+} were rapidly mixed with solutions containing Ca^{2+} and varying concentrations of PS/PC/dPE vesicles under pseudo-first-order conditions. At all the concentrations of vesicles that were tested, the time courses were biphasic (Figure 7A). Visual inspection of residual plots revealed that biexponential equations provided a substantially superior fit over monoexponential equations (Figure 7B,C). The observed rate constant for the

fast phase [$k_{obs(1)}$] was linearly dependent on vesicle concentrations (Figure 7D), whereas that for the slow phase [$k_{obs(2)}$] was approximately hyperbolically dependent (see the inset of Figure 7D). Relative amplitudes of the fast phase were large and approximately hyperbolically dependent on vesicle concentration, whereas those for the slow phase were considerably smaller and flattened out at high vesicle concentrations (Figure 7E) or decreased in some experiments (data not shown). These observations suggest that Ca^{2+}-induced vesicle binding by PKC βII proceeds via two kinetically resolvable steps: a fast phase representing bimolecular association of PKC βII with vesicles and a slow unimolecular transition. In principle, either step may precede the other. Analysis of the fluorescence amplitudes suggests that PKC βII undergoes the unimolecular transition after, but not before, binding membranes (see the Discussion and Supporting Information). This mechanism may be depicted as follows

Scheme 1

$$\text{PKC} + \text{L} \underset{k_{-1}}{\overset{k_1}{\rightleftharpoons}} \text{PKC·L} \underset{k_{-2}}{\overset{k_2}{\rightleftharpoons}} \text{PKC*·L}$$

where PKC*·L represents an altered conformation of the membrane-bound enzyme (PKC·L). For simplicity, this mechanism does not take into consideration rapid Ca^{2+} binding steps; similar results were obtained with or without preincubation of PKC βII with Ca^{2+} prior to rapid mixing (data not shown), suggesting that Ca^{2+} binding to PKC βII is not rate-limiting under these conditions.

Application of equations derived for general two-step mechanisms (25) results in the following approximations for the two phases:

$$k_{obs(1)} \simeq k_1[v] + k_{-1} + k_2 + k_{-2} \qquad (7)$$

$$k_{obs(2)} \simeq \frac{k_1[v](k_2 + k_{-2}) + k_{-1}k_{-2}}{k_1[v] + k_{-1} + k_2 + k_{-2}} \qquad (8)$$

The apparent second-order rate constant for vesicle binding by PKC βII in the bimolecular step, k_1, was estimated from the slope of plots of the vesicle dependence of $k_{obs(1)}$ and equaled 0.61×10^{10} M^{-1} s^{-1} in five independent experiments (Table 3). The y-intercept of this plot provided an estimate for the sum $k_{-1} + k_2 + k_{-2}$ equal to 1.10 s^{-1} (see the legend of Figure 7). The asymptote of the plot of the vesicle dependence of $k_{obs(2)}$ provided an estimate for the sum $k_2 +$
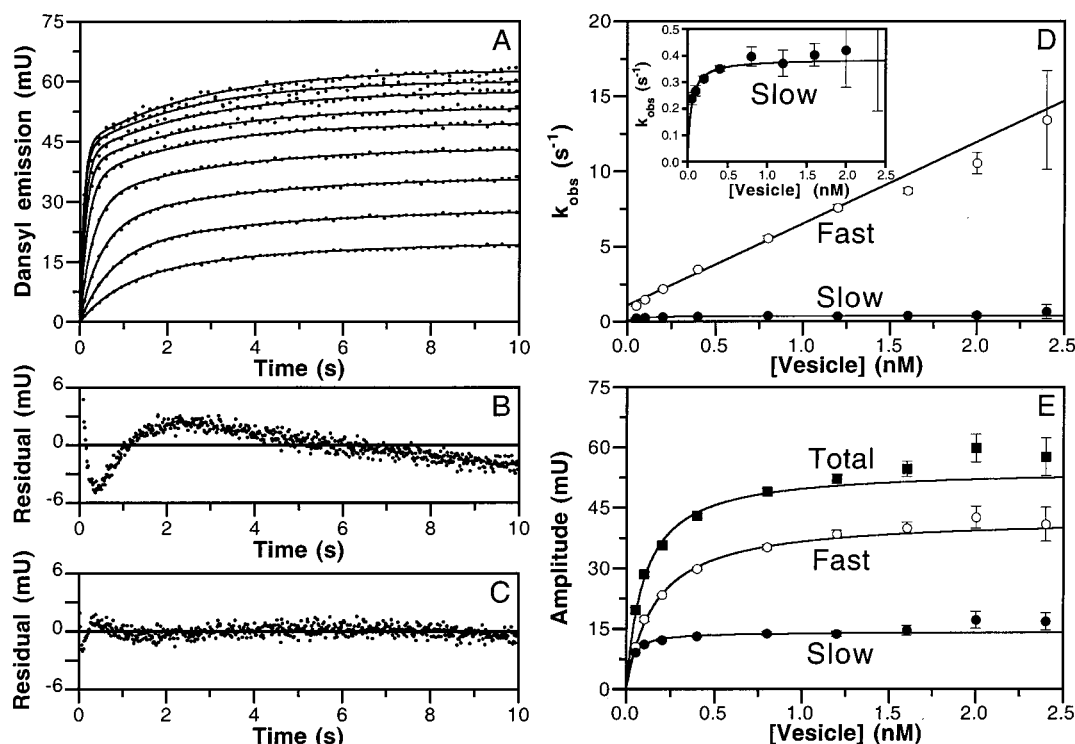
FIGURE 7: Kinetics of Ca^{2+}-triggered PKC βII binding to anionic phospholipid vesicles. Full-length PKC βII (0.2 μM) in Ca^{2+} (200 μM) was rapidly mixed with an equal volume of solutions containing increasing concentrations of PS/PC/dPE (35:60:5) vesicles in Ca^{2+} (200 μM). Tryptophan was excited, and dansyl emission from vesicles was recorded. (A) Representative traces showing the time course of dansyl emission increases for PKC βII mixed with 0.05–2.4 nM (final) vesicles (from bottom to top). Solid lines show biexponential fits, which yielded k_{obs} values and amplitudes for fast and slow phases. (B and C) Representative residual plots from monoexponential (B) or biexponential (C) fits of time courses taken from data employing 1.2 nM vesicles shown in panel A. A poor fit with the monoexponential equation was observed at all vesicle concentrations, whereas the superiority of the biexponential fit was observed at all vesicle concentrations that were tested. (D) Dependence of k_{obs} for fast and slow phases on vesicle concentration. Bars represent standard deviations of three determinations from a single experiment. For the fast phase (O), a solid line shows the weighted linear fit (eq 4), which yielded a slope representing the k_1 value and a y-intercept representing the sum $k_{-1} + k_2 + k_{-2}$. In five independent experiments, the weighted average of k_1 equaled $(0.612 \pm 0.007) \times 10^{10}$ M^{-1} s^{-1} and the weighted average of $k_{-1} + k_2 + k_{-2}$ equaled 1.10 ± 0.03 s^{-1}. For the slow phase ($\bullet$), a solid line shows the weighted hyperbolic fit (eq 5), which yielded an asymptote [$k_{max(2)}$] representing the sum $k_2 + k_{-2}$ equal to 0.68 ± 0.01 s^{-1}. For clarity, the hyperbolic fit of the slow phase is shown in the inset. An estimate for k_{-1} equal to 0.42 ± 0.03 s^{-1} was provided by the difference in the y-intercept of the fast phase ($k_{-1} + k_2 + k_{-2}$) and the asymptote of the slow phase ($k_2 + k_{-2}$). Estimates for the remaining kinetic parameters k_2 and k_{-2} were provided by data described in the legend of Figure 8. (E) Dependence of observed amplitudes for slow ($\bullet$) and fast (O) phases, as well as the total fluorescence change ($\blacksquare$), on vesicle concentration. Bars represent standard deviations of three determinations from a single experiment. The solid line shows a weighted hyperbolic fit (eq 3). From five independent experiments, the hyperbolic fit of the total fluorescence change yielded a weighted average $K_{d(net)}^{obs}$ value for membrane binding equal to 0.119 ± 0.004 nM. Equilibrium and kinetic parameters from this analysis are summarized in Table 3.

Table 3: Equilibrium and Kinetic Parameters of Ca^{2+}-Induced Binding to Anionic Membranes by Full-Length PKC βII

high Ca^{2+} ^{a}							low Ca^{2+} ^{b}
k_1 ($\times 10^{10}$ M^{-1} s^{-1})	k_{-1} (s^{-1})	k_2 (s^{-1})	k_{-2} (s^{-1})	$K_{d(1)}^{calc}$ (nM)	$K_{d(2)}^{calc}$	$K_{d(net)}^{calc}$ (nM)	k_{off} (s^{-1})
0.612 ± 0.007	0.42 ± 0.03	0.44 ± 0.05	0.24 ± 0.05	0.069 ± 0.005	0.56 ± 0.12	0.025 ± 0.006	21 ± 2

^{a} Weighted averages of five independent experiments carried out as described in the legends of Figures 7 and 8, analyzed in terms of Scheme 1, where bimolecular interaction between PKC βII and membrane precedes isomerization. Estimates for k_1 and k_{-1} of the bimolecular step are given in the legend of Figure 7. Estimates for k_2 and k_{-2} of the second step are given in the legend of Figure 8. K_d^{calc} values are defined as the ratio of k_{off} to k_{on} for each step. $K_{d(net)}^{calc}$, which describes the net dissociation constant for both species of membrane-bound PKC βII, was evaluated using eq 10. Experimental conditions: 25 °C, PS/PC/dPE (35:60:5) vesicles, 150 mM NaCl, 20 mM HEPES (pH 7.4), 1 mM DTT, and 200 μM $CaCl_2$. ^{b} Average ($\pm$standard error of the mean) from the Ca^{2+} trapping approach using PS/PC/dPE (35:60:5) vesicles ($n = 8$) (Figure 8B). Experimental conditions (after mixing): 25 °C, 150 mM NaCl, 20 mM HEPES (pH 7.4), 2.5 mM EDTA, 1 mM DTT, 100 μM $CaCl_2$, and 2.4 nM vesicles.

k_{-2}, the maximal rate of the second step, equal to 0.68 s^{-1} (see the legend of Figure 7). The difference in the y-intercept and the asymptote yielded an estimate for k_{-1} equal to 0.42 ± 0.03 s^{-1} (Table 3). The ratio of k_{-1} to k_1 provided an estimate for the K_d^{calc} value of the bimolecular step equal to 0.069 nM (Table 3). Estimates for the remaining rate constants k_2 and k_{-2} were determined by application of a trapping experiment (see below).

Apparent Membrane Dissociation Rate Constants of Full-Length PKC βII. The trapping approaches initially utilized for the C2 domain (Figure 4) were applied to full-length PKC βII (Figure 8). For protein trapping, a solution containing PKC βII preincubated with PS/PC/dPE vesicles and Ca^{2+} was rapidly mixed with a solution containing Ca^{2+} and a large molar excess of unlabeled PS/PC vesicles, and the loss in FRET signal was monitored (Figure 8A). Control experi-
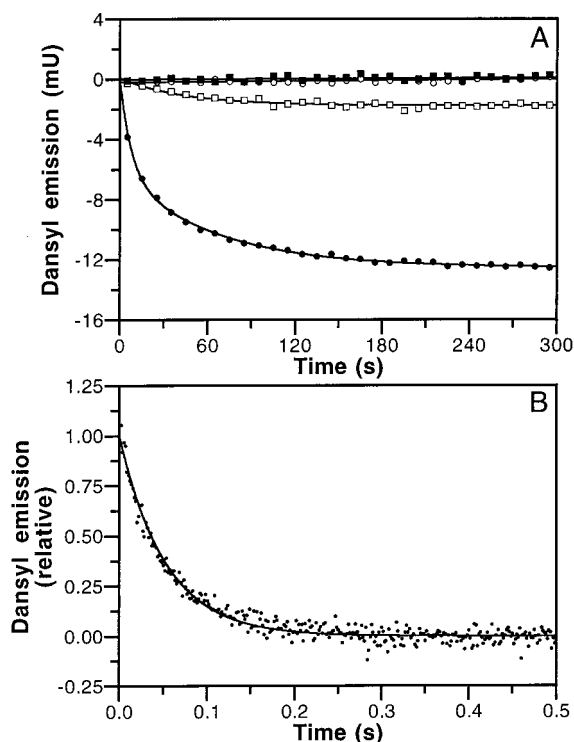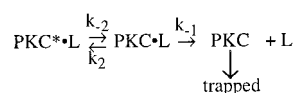
FIGURE 8: Dissociation kinetics of PKC βII measured by trapping. (A) Membrane dissociation kinetics triggered by trapping PKC βII with unlabeled PS/PC vesicles, utilizing tryptophan excitation and dansyl emission. PKC βII (0.2 μM), preincubated with Ca^{2+} (200 μM) and labeled anionic PS/PC/dPE (35:60:5) vesicles (0.2 nM), was rapidly mixed with an equal volume of unlabeled PS/PC (40: 60) vesicles (5 nM) in Ca^{2+} (200 μM) (●). The solid line shows a biexponential fit, which yielded average (±standard error of the mean) values of $k_{off(1)}$ equal to 0.093 ± 0.016 s^{-1} and $k_{off(2)}$ equal to 0.012 ± 0.001 s^{-1} ($n = 6$). The decrease in dansyl emission was eliminated by omitting PKC βII (■) or free Ca^{2+} (○). Substituting the trapping PS/PC vesicles with PS/PC/dPE (35:60: 5) vesicles (0.2 nM) eliminated all but a small monophasic fluorescence decrease (□) that decayed with a rate constant equivalent to $k_{off(2)}$. Therefore, for PKC βII, the apparent dissociation constant was taken to be $k_{off(1)}$ (0.093 s^{-1}). Using eq 9 and the estimates of 1.10 s^{-1} for the sum $k_{-1} + k_2 + k_{-2}$ and 0.42 s^{-1} for k_{-1} (Figure 7), k_{-2} is estimated to be 0.24 ± 0.05 s^{-1}. Using 0.68 s^{-1} as an estimate for the sum $k_2 + k_{-2}$ (Figure 7), k_2 is estimated to be 0.44 ± 0.05 s^{-1}. Deduced estimates for these rate constants are summarized in Table 3. (B) Dissociation of PKC βII from anionic vesicles initiated by rapid Ca^{2+} chelation. PKC βII (0.2 μM), Ca^{2+} (200 μM), and anionic PS/PC/dPE (35:40:5) vesicles (4.8 nM) were rapidly mixed with EDTA (5 mM). Tryptophan was excited, and dansyl emission from vesicles was recorded. Representative trace showing the time course of loss of dansyl emission normalized to the calculated maximal fluorescence change. The solid line shows a monoexponential fit, which yielded an average k_{off} value (±standard error of the mean) of 21 ± 2 s^{-1} ($n = 8$).

ments showed that the observed decrease in dansyl emission required the presence of PKC βII and Ca^{2+}. Since PS/PC vesicles trap the PKC species after its dissociation from PS/ PC/dPE vesicles, the loss in the FRET signal represents the decay in both "visible" species PKC*·L and PKC·L. This trapping procedure may be depicted as follows:

Scheme 1a

$$\text{PKC*·L} \underset{k_2}{\overset{k_{-2}}{\rightleftharpoons}} \text{PKC·L} \overset{k_{-1}}{\rightarrow} \text{PKC} + \text{L}$$
$$\downarrow$$
$$\text{trapped}$$

Depending on the magnitude of the rate constants and whether the equilibrium strongly favors PKC*·L, this trapping procedure may allow measurement of the apparent dissociation constants for both the bimolecular and unimolecular phases. The observed time course of trapping PKC βII by PS/PC vesicles was long (Figure 8A), indicating that the apparent membrane dissociation rate constant of the enzyme is small, and biphasic. Fitting of the data with biexponential equations yielded the following rate constants: $k_{off(1)} = 0.093$ s^{-1} and $k_{off(2)} = 0.012$ s^{-1}. Since control experiments, in which PS/PC vesicles were omitted, demonstrated that only the fast phase represents dissociation of PKC βII triggered by the unlabeled trapping vesicles, the apparent dissociation constant was taken as k_{off}, equal to 0.093 s^{-1}. Mathematically, this apparent dissociation rate constant represents the y-intercept of the plot of the vesicle dependence of $k_{obs(2)}$ depicted by eq 8 (25), which can be approximated by

$$k_{off} \simeq \frac{k_{-1}k_{-2}}{k_{-1} + k_2 + k_{-2}} \tag{9}$$

Using estimates from the analysis provided in Figure 7 for the sum $k_{-1} + k_2 + k_{-2}$ (1.10 s^{-1}) and for k_{-1} (0.42 s^{-1}), k_{-2} was calculated as 0.24 ± 0.05 s^{-1}. Using 0.68 s^{-1} as the estimate for $k_2 + k_{-2}$ (Figure 7D), k_2 therefore equals 0.44 ± 0.05 s^{-1}. Deduced estimates for these rate constants are summarized in Table 3. The ratio of the kinetic constants k_{-2} and k_2 provided an estimate for the K_d^{calc} value of the unimolecular step (0.56). The $K_{d(net)}^{calc}$ value, which describes the net dissociation constant for both species of membrane-bound PKC βII, may be evaluated by (25)

$$K_{d(net)}^{calc} = \frac{K_{d(1)}}{1 + \dfrac{1}{K_{d(2)}}} \tag{10}$$

resulting in a value equal to 0.025 ± 0.006 nM. This value is within a factor of 5 of $K_{d(net)}^{obs}$ (equal to 0.119 nM) evaluated from analysis of the total fluorescence change observed (Figure 7E), indicating relatively good agreement between rate and amplitude data.

Ca^{2+} trapping by EDTA was used to initiate disassembly of the PKC βII−membrane ternary complex, which was monitored by protein-to-membrane FRET (Figure 8B). A solution containing PKC βII, anionic vesicles, and Ca^{2+} was mixed by stopped-flow methods with a solution containing EDTA. The resulting time course was monophasic and yielded a k_{off} value equal to 21 s^{-1} (Table 3). As was the case for the C2 domain, this rate constant for disassembly of the ternary complex at low Ca^{2+} concentrations was considerably larger than the vesicle dissociation constant of 0.093 s^{-1} estimated above in the presence of 200 μM Ca^{2+} (Figure 8A) or the dissociation constant for the bimolecular step represented by the sum $k_{-1} + k_2 + k_{-2}$ (1.10 s^{-1}) (Figure 7D). Thus, the average lifetime of the PKC βII domain− membrane ternary complex is only 48 ms when Ca^{2+} levels are rapidly lowered ($\tau = 1/k_{off} = 1/21$ s^{-1}) but is 11 s in the presence of 200 μM Ca^{2+}.

DISCUSSION

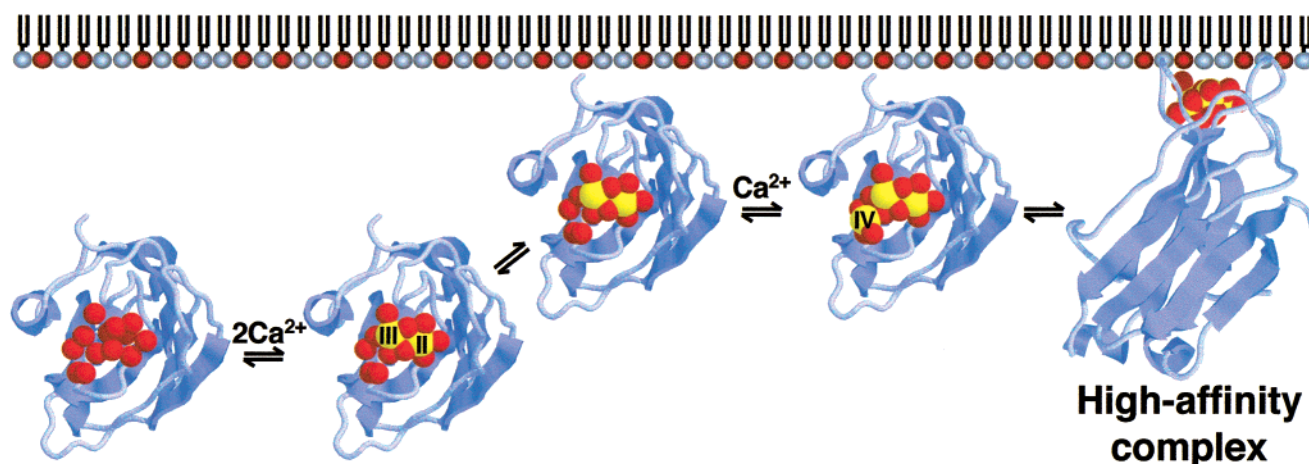This study dissects how Ca^{2+} modulates the rate constants of anionic membrane binding by the PKC β C2 domain,

FIGURE 9: Proposed mechanism for C2 domain binding to anionic membranes induced by Ca^{2+}. Ribbon representation of the PKC β C2 domain (*32*), indicating Ca^{2+} coordinating oxygen ligands (red spheres) and bound Ca^{2+} ions (yellow spheres). In the absence of Ca^{2+}, the affinity of the C2 domain for membranes is low because of unfavorable electrostatic interactions. When Ca^{2+} levels rise, two Ca^{2+} ions (II and III) bind to the free domain. The $C2 \cdot Ca_2$ species binds randomly to the phospholipid surface, forming a low-affinity domain−membrane encounter complex, whose lifetime is prolonged (compared to that of the $C2 \cdot Ca_0 \cdot$membrane complex) by favorable electrostatic interactions. Binding of the third Ca^{2+} ion (IV) results in formation of a high-affinity C2 domain−membrane ternary complex, where Ca^{2+} ions act as a bridge and residues in the Ca^{2+}-binding loops insert into the lipid bilayer.

either alone or in the context of full-length PKC βII. Previous studies have established that Ca^{2+} dramatically increases the affinity of PKC for anionic membranes (*22, 24, 26*). Here we show that Ca^{2+} binds to the free C2 domain with relatively low affinity ($K_d \sim 55\ \mu M$) and that Ca^{2+} binding both increases the apparent association rate constant (k_{on}) and decreases the apparent dissociation rate constant (k_{off}) for membrane binding, thus prolonging its lifetime on the membrane. Both binding constants are sensitive to the anionic phospholipid content and Mg^{2+} concentration; increasing the PS mole fraction or decreasing the Mg^{2+} concentration elevates the apparent affinity of the C2 domain for membranes by simultaneously increasing k_{on} and decreasing k_{off} for membrane binding. Furthermore, rapid lowering of the Ca^{2+} concentration results in a marked increase in k_{off}, an increase that is unaffected by the PS mole fraction or Mg^{2+} concentration. Ca^{2+}-dependent binding of full-length PKC to membranes also proceeds by a bimolecular reaction but differs from that of the isolated domain in that binding consists of two kinetically resolvable components. These two components reflect rapid bimolecular interaction with the membrane and, most likely, the previously described conformational change that accompanies membrane binding (*27*). As is the case for the C2 domain, the k_{off} of full-length PKC βII increases by several orders of magnitude when free Ca^{2+} is rapidly removed. Thus, Ca^{2+} dictates how rapidly PKC binds membranes and how long the enzyme is retained on the membrane.

Ca^{2+} Binding to the Isolated PKC β C2 Domain in the Absence of Membranes. The results presented here and previous results (*17*) suggest that two or more Ca^{2+} ions bind rapidly to the free PKC β domain in solution (Figure 9), which may be depicted simplistically as follows:

Scheme 2

$$C2 + nCa \underset{k_{off(Ca)}}{\overset{k_{on(Ca)}}{\rightleftharpoons}} C2 \cdot Ca_n$$
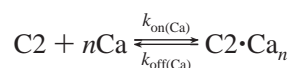
where $n \geq 2$ and $k_{on(Ca)}$ and $k_{off(Ca)}$ represent net second-order association and dissociation rate constants, respectively.

Our results demonstrate that even at low micromolar Ca^{2+} concentrations, this binding reaction is complete within 2 ms, an upper limit defined by the physical specifications of the stopped-flow apparatus. As reported here and elsewhere (*17*), $k_{off(Ca)}$ is estimated to be very large ($\gg 500\ s^{-1}$). Thus, for a Ca^{2+} dissociation constant of approximately 55 μM (Figure 1B) and a $k_{off(Ca)}$ of $\gg 500\ s^{-1}$, the apparent $k_{on(Ca)}$ for the free PKC β C2 domain in solution is at least 1×10^7 $M^{-1}\ s^{-1}$, a value comparable to that reported for many other Ca^{2+}-binding proteins (*28, 29*).

The binding of two Ca^{2+} ions to the free PKC β C2 domain achieved in the presence of 200 μM Ca^{2+} measured here and elsewhere (*17*) is consistent with NMR studies of the domain (*30*) and crystallographic structure determination of the PKC α C2 domain bound with two Ca^{2+} ions (*31*). These two ions represent Ca^{2+} ions II and III, using a standardized numbering system (*32*). The third ion present in crystals of PKC β C2 domain dimers, which represents Ca^{2+} ion IV, is likely to bind monomers with extremely low affinity in solution but becomes trapped in the crystallographic dimer interface or, physiologically, in a ternary C2 domain−membrane complex (*32*). In principle, this third Ca^{2+} ion may be stabilized in the ternary complex by oxygens provided by phospholipid headgroups or adjacent domains in the full-length enzyme, including phosphate oxygens provided by phosphoserine-660 in the C-terminal tail of PKC βII (see below).
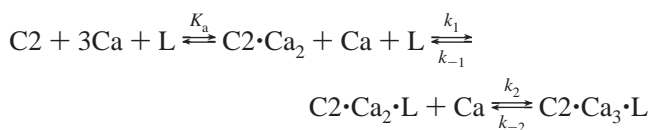
Ca^{2+}-Induced Membrane Binding by the Isolated PKC β C2 Domain. In the presence of 200 μM Ca^{2+}, >90% of the PKC β C2 domain is bound with two or more Ca^{2+} ions, based on a Hill coefficient of 1.9 and the $[Ca^{2+}]_{1/2}$ value of 55 μM (Figure 1). At this Ca^{2+} concentration, the time course of membrane binding by the C2 domain consists of a single phase with an observed rate constant that increases linearly with vesicle concentration up to 2.4 nM vesicles without signs of curvature. These results suggest that Ca^{2+}-induced binding of the C2 domain to anionic phospholipids proceeds via a simple bimolecular interaction between the $C2 \cdot Ca_n$ species and the vesicle, where n reflects the ambiguity in the Ca^{2+} stoichiometry prior to the encounter between the

domain and the membrane (addressed below). The rate of binding is limited by the rate of collision between the vesicle and the C2 domain and not by Ca^{2+} binding, which is rapid. The failure to observe curvature in plots of k_{obs} versus vesicle concentration suggests that the initial binding of vesicles with the $C2 \cdot Ca_n$ species is weak. The estimated dissociation constant for this weak interaction, based on vesicle concentration, is >48 nM, a value that is considerably larger than the net dissociation constant calculated to be 0.73 nM.

In the presence of 2.4 nM vesicles, the apparent membrane affinity of the C2 domain increases with Ca^{2+} concentration because of both a decrease in k_{off} and an increase in k_{on}. Simulating a rapidly decaying Ca^{2+} signal, the Ca^{2+} trapping experiment demonstrated that the k_{off} for the C2 domain—membrane complex is large, 150 s^{-1}, when Ca^{2+} levels are low. Conversely, simulating a sustained Ca^{2+} signal, the C2 domain trapping experiment demonstrated that the k_{off} value is approximately 20-fold smaller, 9.2 s^{-1}, in the presence of 200 μM Ca^{2+}. Furthermore, when the bulk Ca^{2+} concentration is increased from 50 to 200 μM, k_{off} decreases from 16 to 8.9 s^{-1} and k_{on} increases from 0.73 × 10^{10} to 1.2 × 10^{10} M^{-1} s^{-1}. Together, these results suggest that at low Ca^{2+} concentrations, C2 domain binding to membranes is weak due to a very large k_{off} value and a low basal k_{on}.

To account for these effects on the observed rate constants, we propose the following model. In the presence of 200 μM Ca^{2+}, two Ca^{2+} ions, II and III, initially bind rapidly to the free domain to form $C2 \cdot Ca_2$. Then, contact between the domain and the vesicle results in formation of a (hypothetical) unstable domain—membrane encounter complex ($C2 \cdot Ca_2 \cdot L$), which is held together by nonspecific electrostatic interactions (discussed in greater detail below). Subsequently, rapid binding of the third Ca^{2+} ion, IV, to this intermediate leads to formation of the high-affinity ternary complex ($C2 \cdot Ca_3 \cdot L$). This mechanism may be depicted as follows:

Scheme 3

$$C2 + 3Ca + L \underset{}{\overset{K_a}{\rightleftharpoons}} C2 \cdot Ca_2 + Ca + L \underset{k_{-1}}{\overset{k_1}{\rightleftharpoons}}$$

$$C2 \cdot Ca_2 \cdot L + Ca \underset{k_{-2}}{\overset{k_2}{\rightleftharpoons}} C2 \cdot Ca_3 \cdot L$$

where K_a represents the average affinity of the first two Ca^{2+} ions, k_1 and k_{-1} represent the forward and reverse rate constants for formation of a $C2 \cdot Ca_2 \cdot L$ encounter complex, respectively, and k_2 and k_{-2} represent the net rate constants for the binding of the third Ca^{2+} ion and final rearrangement to the high-affinity ternary complex, respectively. Importantly, the binding affinity of the third Ca^{2+} ion is too low to promote occupancy except when Ca^{2+} levels reach into the millimolar range or additional groups for Ca^{2+} coordination are provided, as in the presence of phospholipid. This model is depicted in Figure 9.

According to this model, the apparent rate constants k_{on} and k_{off} represent complex functions of these hypothetical fundamental rate constants (25). These relationships can account for the observation that as the Ca^{2+} concentration is elevated, both k_{on} increases and k_{off} decreases (E. A. Nalefski, manuscript in preparation). These effects may be due to (i) prolongation of the lifetime of the $C2 \cdot Ca_2 \cdot L$ encounter complex by a reduction in k_{-1} or (ii) acceleration in the rate of formation of the high-affinity $C2 \cdot Ca_3 \cdot L$ ternary complex by an increase in k_2. When Ca^{2+} levels are rapidly

lowered (as in the Ca^{2+} trapping experiment), the rate of release of the domain from the membrane appears to be limited by the net rate of dissociation of at least one Ca^{2+} ion, presumably IV; i.e., $k_{-2} \ll k_{-1}$. Consequently, k_{off} simplifies to k_{-2}, which may be estimated to be ~150 s^{-1}. Thus, the data presented here are consistent with a mechanism involving the binding of at least one Ca^{2+} ion after the initial encounter of the domain with membranes and rule out an alternative mechanism involving the binding of all three Ca^{2+} ions prior to the initial contact.

Effects of PS Percentage and the Presence of Mg^{2+}. Reducing the magnitude of the membrane surface potential by lowering the membrane PS mole fraction, including 5 mM MgCl$_2$ in the binding reaction, or increasing the ionic strength of the binding reaction mixture (data not shown) results in reduction of the apparent membrane affinity of the PKC β C2 domain measured in the presence of 200 μM Ca^{2+}. In each case, this reduction results from both an increase in k_{off} and a decrease in k_{on}. Therefore, decreasing the magnitude of the surface potential might lower the affinity of the C2 domain for membranes by influencing the rate constants for hypothetical steps in a manner similar to that with reduction of Ca^{2+} concentrations. Alternatively, k_{off} may increase indirectly from a reduction of the Ca^{2+} concentration near the vesicle surface as a result of a decrease in the magnitude of the membrane surface potential. Likewise, a decrease in k_{on} may be ascribed to direct or indirect effects on rates of binding.

Trapping studies provide further insight into the effects of the membrane surface potential on the membrane interaction of the C2 domain. When free Ca^{2+} levels are rapidly lowered in Ca^{2+} trapping experiments, both the PS mole fraction and the presence of Mg^{2+} have little effect on k_{off}. Thus, these observations suggest that favorable electrostatic interactions decrease k_{off} mainly by stabilizing the hypothetical $C2 \cdot Ca_2 \cdot L$ encounter complex, via increasing its lifetime, or by increasing the rate of its transformation to the $C2 \cdot Ca_3 \cdot L$ complex. Likewise, these effects can account for the observed increases in k_{on} for binding of the PKC β C2 domain to anionic vesicles by favorable electrostatic interactions. Nonspecific electrostatic interactions may serve to promote Ca^{2+} binding to an otherwise low-affinity site or to prolong the lifetime of the initial domain—membrane encounter complex, both of which increase the likelihood that the C2 domain will undergo final rearrangement to form a high-affinity complex.

Together, these results provide a deeper molecular understanding for the widely recognized finding that favorable electrostatic interactions promote binding of the PKC C2 domain to anionic membranes (3, 17, 33, 34). The increase in the lifetime of the hypothetical $C2 \cdot Ca_2 \cdot L$ encounter complex by both favorable electrostatic interactions and Ca^{2+} is consistent with the hypothesis that Ca^{2+} acts as an electrostatic switch, inducing a large change in electrostatic potential to drive interactions with oppositely charged, anionic phospholipid membranes (39). Equally likely is the possibility that formation of the Ca^{2+} bridge between the domain and membrane (31) further accelerates the insertion of several hydrophobic groups of the domain into the lipid bilayer (33). The requirement for such a bridge accounts for why neutralization of the Ca^{2+} binding site of the PKC βII C2 domain did not mimic the effect of Ca^{2+} in recruiting this enzyme to membranes (35). Favorable electrostatic

interactions have been demonstrated to accelerate rates of many specific binding interactions (*36*, *37*). It is anticipated that these principles will be applicable to other C2 domains, such as those in the synaptic vesicle protein synaptotagmin, whose binding to anionic phospholipid membranes is also enhanced by electrostatic interactions (*17*, *38*, *39*).

Ca²⁺-Induced Membrane Binding by Full-Length PKC βII. Stopped-flow analysis revealed that the membrane binding reaction of PKC βII is considerably more complex than that of its isolated C2 domain. Specifically, the reaction is composed of two kinetically resolvable phases, one representing the rapid bimolecular association of the enzyme with the vesicle and the other representing a slow first-order transition (Scheme 1). These steps likely represent the rapid binding of PKC to the anionic membrane surface via the C2 domain and a slow conformational change in the enzyme. Analysis of amplitudes from the time courses suggests that the slow conformational change follows, rather than precedes, membrane binding. In comparison to such an alternative mechanism, the preferred mechanism (Scheme 1) provided closer agreement between the estimate of the dissociation constant for the bimolecular step based on observed fluorescence amplitudes and that calculated from rate constants (see the Supporting Information). We assume that, as is the case for the isolated C2 domain, Ca²⁺-binding steps are rapid and not rate-limiting.

Comparison of the equilibrium and kinetic parameters of the bimolecular step for full-length PKC βII to those of the isolated C2 domain suggests that the membrane binding properties of the domain in the full-length enzyme are influenced by physical features outside the C2 domain. For instance, the dissociation rate constant for the bimolecular step of the full-length enzyme (0.42 s⁻¹) is 20-fold smaller than that for the isolated C2 domain (8.9 s⁻¹), indicating that the higher membrane affinity of the full-length enzyme stems primarily from its decreased apparent dissociation rate constant. This decrease indicates that regions outside the C2 domain, such as the C1 domain or the C-terminus, may provide additional favorable interactions with the membrane surface or may influence the properties of the C2 domain. Specifically, since the affinity of the C1 domain for membranes containing DG is greatly enhanced by an increased PS mole fraction and electrostatic interactions (*3*, *34*, *40*), the C1 domain may provide an additional point of contact with the membrane even in the absence of DG. Alternatively, the C-terminal tail of PKC β, in particular phosphoserine-660, has been shown to modulate the Ca²⁺ sensitivity for binding of the full-length enzyme to anionic membranes (*41*). Furthermore, Ca²⁺ ions bound in the C2 domain−membrane ternary complexes of the full-length enzyme may be more fully liganded than those of the isolated domain (*32*), which is likely to, in turn, further decrease the apparent membrane dissociation rate constant. On the other hand, the apparent association constant for binding the full-length enzyme in the bimolecular step (0.61×10^{10} M⁻¹ s⁻¹) is approximately half that for the isolated C2 domain (1.2×10^{10} M⁻¹ s⁻¹). Most of this reduction may be attributed to the smaller diffusion constant of the full-length enzyme as a consequence of its larger size (E. A. Nalefski, manuscript in preparation). These results suggest that the enzyme does not undergo a slow obligatory conformational change to unmask the C2 domain prior to membrane binding, as has been reported for the C1 domain of PKC γ (*6*).
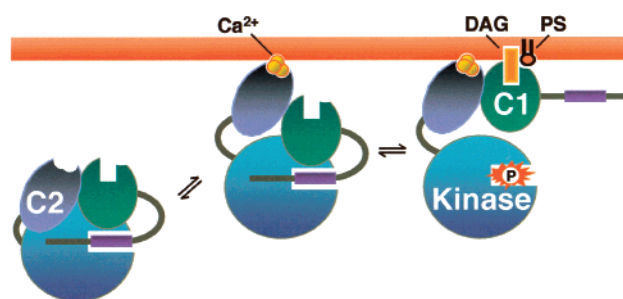

FIGURE 10: Proposed role of the C2 domain in PKC in facilitating the search for DG. The binding of Ca²⁺ (yellow) to the C2 domain (blue) results in nonspecific association of PKC near the diffusion-controlled limit with anionic phospholipids commonly found in the inner leaflet of cellular membranes. This reduces the dimensionality of the search for DG (orange) by the C1 domain (green) to the plane of the membrane, increasing the efficiency of PKC in finding this rare membrane constituent. Once the C1 domain engages DG and PS, a conformational change releases the autoinhibitory pseudosubstrate (deep purple) from the catalytic site, thus activating the enzyme.

By analogy to the hypothetical binding steps postulated for the C2 domain, dissociation of the full-length enzyme may be limited by the net rate of Ca²⁺ release from the protein. The apparent dissociation rate constant measured when Ca²⁺ levels are rapidly lowered (21 s⁻¹) is 7-fold smaller than the corresponding rate constant for the isolated C2 domain (150 s⁻¹). As proposed above, this may indicate that additional contacts between the enzyme and membrane must be broken or that a conformational change must take place before Ca²⁺ can be released. Importantly, these results indicate that, as is the case for the isolated C2 domain, the enzyme remains bound to the membrane for prolonged periods of time when elevated Ca²⁺ levels are sustained ($\tau \sim 11$ s) but is rapidly released when Ca²⁺ levels are suddenly reduced ($\tau \sim 48$ ms). Together, these features might enable the enzyme to faithfully track Ca²⁺ spikes resolved by at least 50 ms. Indeed, PKC γ has been shown to rapidly dissociate from plasma membranes upon termination of Ca²⁺ spikes (*6*).

Although the exact nature of the slow conformational change in the membrane-bound enzyme remains to be fully characterized, it does not appear to be very energetically favorable. The K_a for this step is less than 2, calculated as the ratio of k_2 to k_{-2} (Table 3). This conformational change may represent one that increases the level of exposure of a proteolytic site in the hinge region that separates the C2 and catalytic domains, observed specifically when PKC enzymes engage membranes through their C2 domains (*27*). Alternatively, the conformational change may reflect reorientation of the C1 domain with respect to the membrane. Since the apparent dissociation rate constant of the full-length enzyme at low Ca²⁺ concentrations is considerably larger than that in the presence of 200 µM Ca²⁺, the conformational change itself may be driven forward by Ca²⁺ binding and may decay reversibly via a fast step involving the release of Ca²⁺. Further experiments will be required to characterize this conformational change and its relationship to the mechanism of PKC activation.

Model. Analysis of the association and dissociation rate constants of the isolated C2 domain and of full-length PKC is consistent with the model for the regulation of PKC by Ca²⁺ (Figure 10). In the absence of Ca²⁺, PKC collides with membranes at the diffusion-controlled limit but rapidly

dissociates because unfavorable electrostatic interactions between the C2 domain and the anionic membrane surface shorten the lifetime of the encounter complex. Hence, the apparent affinity is too low for significant binding; on the basis of a K_a for lipid of $<10^2$ M^{-1} (3), the estimated K_d for this interaction is greater than 100 nM in terms of vesicle concentration (assuming 9×10^4 lipids per vesicle). Following elevation of intracellular Ca^{2+}, the C2 domain binds Ca^{2+} ions with relatively low affinity. This Ca^{2+}-bound species has a significantly higher affinity for membranes resulting from an increase in k_{on} and a decrease in k_{off}. Once recruited to the membrane, a third Ca^{2+} ion binds, stabilizing the C2 domain−membrane complex. The increased residency time of this complex allows PKC to search two-dimensional space for the C1 domain ligand, DG, as long as Ca^{2+} levels remain elevated. Once the C1 domain engages membranes through DG and PS, the autoinhibitory pseudosubstrate is expelled from the catalytic site, activating the enzyme.

Conclusions. The results presented in this study illustrate how favorable electrostatic interactions participate in driving the association of the PKC β C2 domain with anionic phospholipid membranes. Rapid Ca^{2+} binding to the domain enhances the affinity of the domain for membranes by elevating the low basal k_{on} for binding and by reducing k_{off}. Similarly, increasing the magnitude of the membrane surface potential elevates k_{on} and reduces k_{off}. Acceleration of the rate of binding thus appears to be enhanced by favorable electrostatic interactions, enabling the C2 domain to bind nonspecifically to anionic phospholipids common in the inner leaflet of cellular membranes at the diffusion-controlled limit. Full-length PKC βII also binds near the diffusion-controlled limit to anionic membranes via the C2 domain. However, an additional conformational change ensues upon membrane binding, thus prolonging the lifetime of the enzyme−membrane complex in both the presence and absence of Ca^{2+}. We anticipate that Ca^{2+}-independent isoforms of PKC might display a reduced k_{on}, reflecting the inability of Ca^{2+} to enhance the specific rate of membrane association.

ACKNOWLEDGMENT

SUPPORTING INFORMATION AVAILABLE

Consideration of an alternative mechanism and equilibrium and kinetic parameters of Ca^{2+}-induced binding of full-length PKC βII to anionic membranes. This material is available free of charge via the Internet at http://pubs.acs.org.

REFERENCES

1. Hurley, J. H., and Misra, S. (2000) *Annu. Rev. Biophys. Biomol. Struct. 29*, 49−79.
2. Newton, A. C., and Johnson, J. E. (1998) *Biochim. Biophys. Acta 1376*, 155−172.
3. Johnson, J. E., Giorgione, J., and Newton, A. C. (2000) *Biochemistry 39*, 11360−11369.
4. Sakai, N., Sasaki, K., Ikegaki, N., Shirai, Y., Ono, Y., and Saito, N. (1997) *J. Cell Biol. 139*, 1465−1476.
5. Feng, X., Zhang, J., Barak, L. S., Meyer, T., Caron, M. G., and Hannun, Y. A. (1998) *J. Biol. Chem. 273*, 10755−10762.
6. Oancea, E., and Meyer, T. (1998) *Cell 95*, 307−318.
7. Ohmori, S., Shirai, Y., Sakai, N., Fujii, M., Konishi, H., Kikkawa, U., and Saito, N. (1998) *Mol. Cell. Biol. 18*, 5263−5271.
8. Maasch, C., Wagner, S., Lindschau, C., Alexander, G., Buchner, K., Gollasch, M., Luft, F. C., and Haller, H. (2000) *FASEB J. 14*, 1653−1663.
9. Vallentin, A., Prevostel, C., Fauquier, T., Bonnefont, X., and Joubert, D. (2000) *J. Biol. Chem. 275*, 6014−6021.
10. Wagner, S., Harteneck, C., Hucho, F., and Buchner, K. (2000) *Exp. Cell. Res. 258*, 204−214.
11. Berridge, M. J. (1990) *J. Biol. Chem. 265*, 9583−9586.
12. Werner, M. H., Bielawska, A. E., and Hannun, Y. A. (1992) *Biochem. J. 282*, 815−820.
13. Mosior, M., and Newton, A. C. (1995) *J. Biol. Chem. 270*, 25526−25533.
14. Bartlett, G. R. (1958) *J. Biol. Chem. 234*, 466−468.
15. Arbuzova, A., Wang, J., Murray, D., Jacob, J., Cafiso, D. S., and McLaughlin, S. (1997) *J. Biol. Chem. 272*, 27167−27177.
16. Nalefski, E. A., and Falke, J. J. (2001) in *Methods in Molecular Biology* (Vogel, H. J., Ed.) Humana Press, Totowa, NJ (in press).
17. Nalefski, E. A., Wisner, M. A., Chen, J. Z., Sprang, S. R., Fukuda, M., Mikoshiba, K., and Falke, J. J. (2001) *Biochemistry 40*, 3089−3100.
18. Orr, J. W., and Newton, A. C. (1992) *Biochemistry 31*, 4661−4667.
19. Tonomura, B., Nakatani, H., Ohnishi, M., Yamaguchi-Ito, J., and Hiromi, K. (1978) *Anal. Biochem. 84*, 370−383.
20. Taylor, J. R. (1997) *An Introduction to Error Analysis*, 2nd ed., University Science Books, Sausalito, CA.
21. Nalefski, E. A., Slazas, M. M., and Falke, J. J. (1997) *Biochemistry 36*, 12011−12018.
22. Mosior, M., and Epand, R. M. (1994) *J. Biol. Chem. 269*, 13798−13805.
23. McLaughlin, S. (1989) *Annu. Rev. Biophys. Biophys. Chem. 18*, 113−136.
24. Mosior, M., and Epand, R. M. (1993) *Biochemistry 32*, 66−75.
25. Johnson, K. A. (1992) in *Methods in Enzymology* (Sigman, D. S., Ed.) pp 1−61, Harcourt Brace Jovanovich, San Diego.
26. Bazzi, M. D., and Nelsestuen, G. L. (1987) *Biochemistry 26*, 115−122.
27. Keranen, L. M., and Newton, A. C. (1997) *J. Biol. Chem. 272*, 25959−25967.
28. Falke, J. J., Drake, S. K., Hazard, A. L., and Peersen, O. B. (1994) *Q. Rev. Biophys. 27*, 219−290.
29. Linse, S., and Forsen, S. (1995) *Adv. Second Messenger Phosphoprotein Res. 30*, 89−151.
30. Shao, X., Davletov, B. A., Sutton, R. B., Sudhof, T. C., and Rizo, J. (1996) *Science 273*, 248−251.
31. Verdaguer, N., Corbalan-Garcia, S., Ochoa, W. F., Fita, I., and Gomez-Fernandez, J. C. (1999) *EMBO J. 18*, 6329−6338.
32. Sutton, R. B., and Sprang, S. R. (1998) *Structure 6*, 1395−1405.
33. Medkova, M., and Cho, W. (1998) *J. Biol. Chem. 273*, 17544−17552.
34. Medkova, M., and Cho, W. (1999) *J. Biol. Chem. 274*, 19852−19861.
35. Edwards, A. S., and Newton, A. C. (1997) *Biochemistry 36*, 15615−15623.
36. Honig, B., and Nicholls, A. (1995) *Science 268*, 1144−1149.
37. Schreiber, G., and Fersht, A. R. (1996) *Nat. Struct. Biol. 3*, 427−431.
38. Chapman, E. R., and Davis, A. F. (1998) *J. Biol. Chem. 273*, 13995−14001.
39. Zhang, X., Rizo, J., and Sudhof, T. C. (1998) *Biochemistry 37*, 12395−12403.
40. Bittova, L., Stahelin, R. V., and Cho, W. (2001) *J. Biol. Chem. 276*, 4218−4226.
41. Edwards, A. S., and Newton, A. C. (1997) *J. Biol. Chem. 272*, 18382−18390.